The CLAS Čerenkov Detector

G. Adams [a], V. Burkert [c], T. Carstens [c], V. Frolov [a]
L. Houghtlin [a] G. Jacobs [c], M. Kossov [c], M. Klusman [a],
B. Kross [c], M. Onuk [a] J. Napolitano [a], J.W. Price [a], C. Riggs [c],
M. Kossov [b], Y. Sharabian [d], A. Stavinsky [b], L.C. Smith [e]
P. Stoler [a], W. Tuzel, [c], K. Ullrich [a] A. Vlassov, [b],
A. Weisenberger, [c] M. Witkowski, [a], B. Wojtekhowski, [a]
P.F. Yergin, [a] C. Zorn. [c]

[a] *Department of Physics, Rensselaer Polytechnic Institute, Troy, NY 12180*

[b] *Institute For Theoretical & Experimental Physics, Moscow, Russia*

[c] *Thomas Jefferson National Accelerator Facility, Newport News, VA 23606*

[d] *Yerevan Physics Institute, Yerevan, Armenia*

[e] *Physics Department, Univ. of Virginia, Charlottesville, VA*

Abstract

The design, construction, and performance of the CLAS Čerenkov thereshold gas detector at Jefferson Lab. is described. The detector consists of 216 optical modules. Each module consists of 3 adjustable mirrors, of lightweight composite construction, a Winston light collecting cone, a 5-inch photomultiplier tube, and specially designed magnetic shielding.

PACS No. 95.55.Vj

Keywords: Detector, Čerenkov, gas, threshold

Preprint submitted to Elsevier Preprint *8 August 2000*

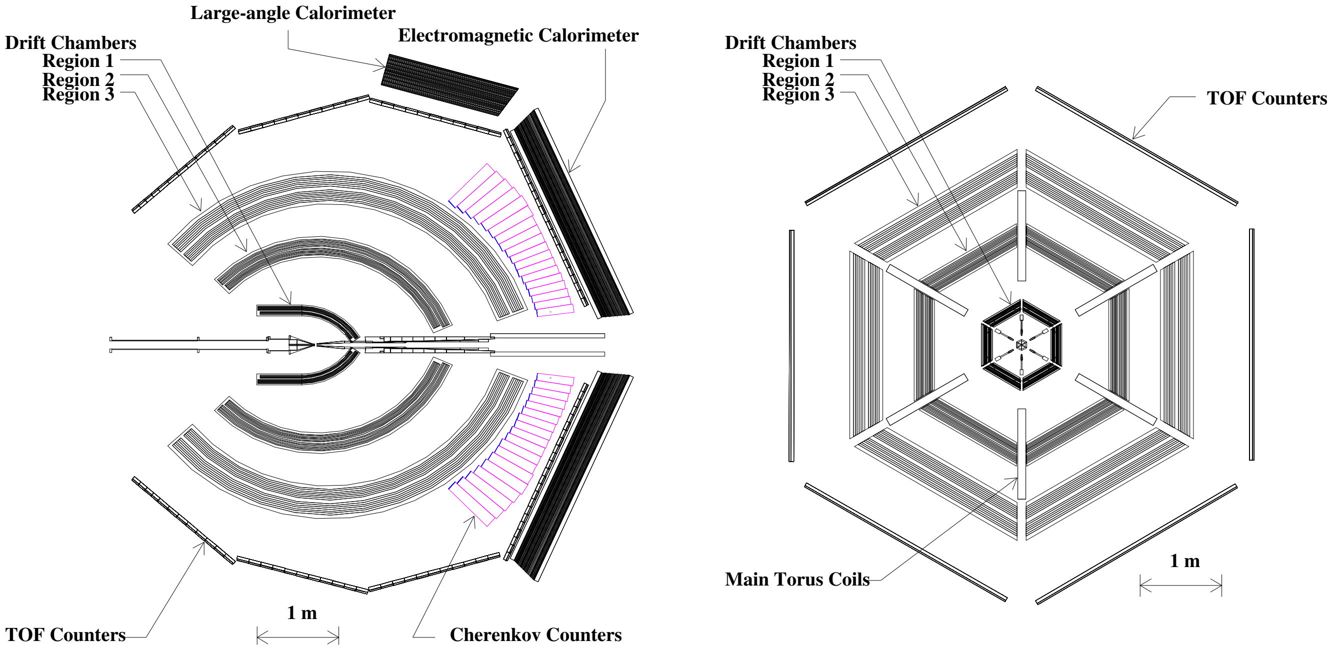

Fig. 1. A schematic drawing of the CLAS detector showing, on the left a vertical section along the beam line, and on the right a section through the target position normal to the beam line.

1 Introduction

The CEBAF Large Acceptance Spectrometer (CLAS) is a nearly-4π detector at the Thomas Jefferson National Accelerator Facility for the study of electromagnetic interactions with nucleons and nuclei. Figure 1 schematically shows the CLAS and the placement of the various detector components.

Six superconducting coils produce a toroidal magnetic field having six-fold symmetry around the beam axis, in which charged particles are bent in θ while their ϕ direction remains largely unaffected. Tracking is accomplished in three drift chamber regions, containing a total of 18 axial and 16 stereo layers of drift cells. These are followed by gas Čerenkov detectors, scintillation detectors, and electromagnetic calorimeters for particle identification and timing. The Čerenkov detectors serve the functions of triggering on electrons, and separating electrons from pions. The unique space and geometry constraints within the CLAS spectrometer require a Čerenkov detector with unusual optical and physical design characteristics.

2 Cerenkov Design

The approximately toroidal magnetic field is provided by six superconducting coils spaced by angles of 60° in ϕ, where ϕ is the azimuthal angle around the electron beam. In order to minimize hadron and electron absorption, and secondary particle production upstream of the time of flight scintillators and calorimeters, it is necessary to minimize the amount of material in all of the preceding detectors. This places stringent requirements on the physical properties of the Čerenkov detector.

The design of the Čerenkov detector aims at maximizing the coverage in each of the six sectors out to an angle $\theta = 45°$. This is done by covering as much of the available space as possible with mirrors, and placing the light collecting cones and photomultiplier tubes (PMTs) in the regions of ϕ which are obscured by the magnet coils.

Due to the approximately toroidal configuration of the magnetic field, the charged particle trajectories take place approximately in planes of constant ϕ. This suggested that the light collection optics be designed to focus the light in the ϕ direction. To this end, each of the six sectors was divided into 18 regions of θ, and each θ segment was divided into two modules about the symmetry plane bisecting each sector. This results in a total of 12 identical (except for an inversion symmetry) subsectors around the ϕ direction for each θ interval, and a total of 216 light collection modules.

The optics of each θ module was designed to focus the light onto a photomultiplier tube (PMT) associated with that module and located in the region obscured by the coils. Figure 2 shows the optical arrangement of one module. The array of the modules in one sector is shown in Figure 3. The optical elements of each module consist of two focussing mirrors, a "Winston" light collection cone, and cylindrical mirror at the base of the cone as shown in Figure 2. The light detection is done by means of a 5 inch Phillips XP4500B PMT mounted at the base of the Winston cone.

The trajectory of the light produced by a typical electron passing through the Čerenkov detector is also illustrated in Figure 2. Since the distance between coils increases linearly with θ, each of the 18 modules in θ has unique optical design parameters.

2.1 Photomultiplier Tubes.

Monte-Carlo simulation showed that at extreme but important regions of the angular acceptance of the spectrometer the number of detected photoelectrons is rather low. In order to maintain acceptable detection efficiency in these regions, stringent requirements, within budgetary constraints, were placed on the photomultiplier performance. In order to trigger

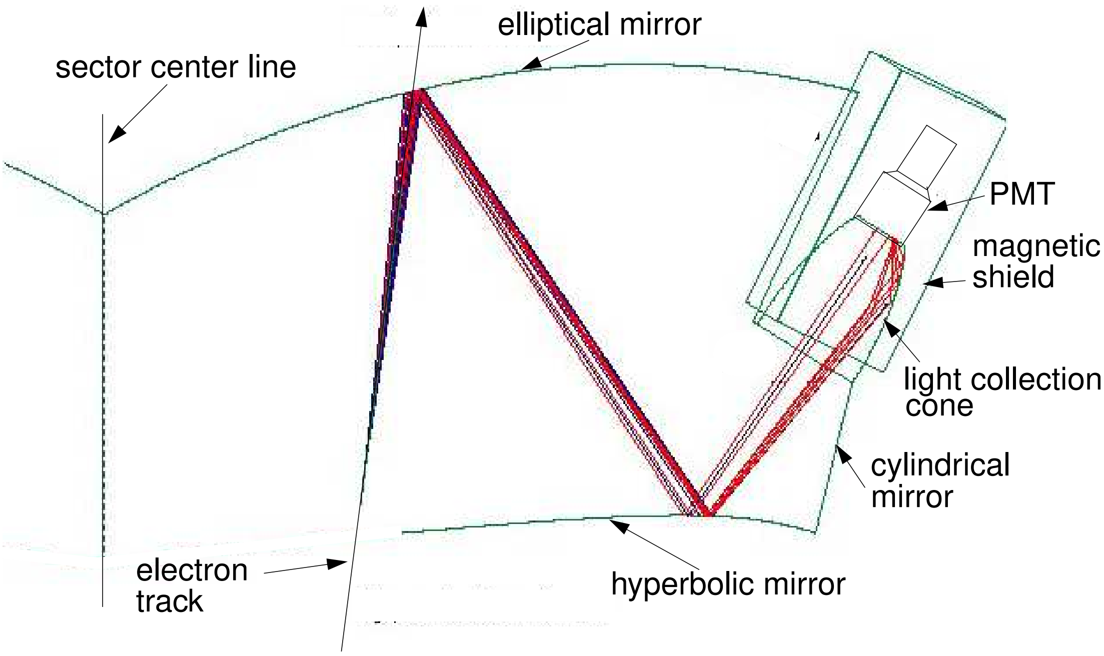

Fig. 2. Optical arrangement of one of 216 optical modules of the CLAS Čerenkov detector, showing the optical and light collection componants. Note that the Čerenkov PMTs lie in the ϕ region obscured by the magnet coils.

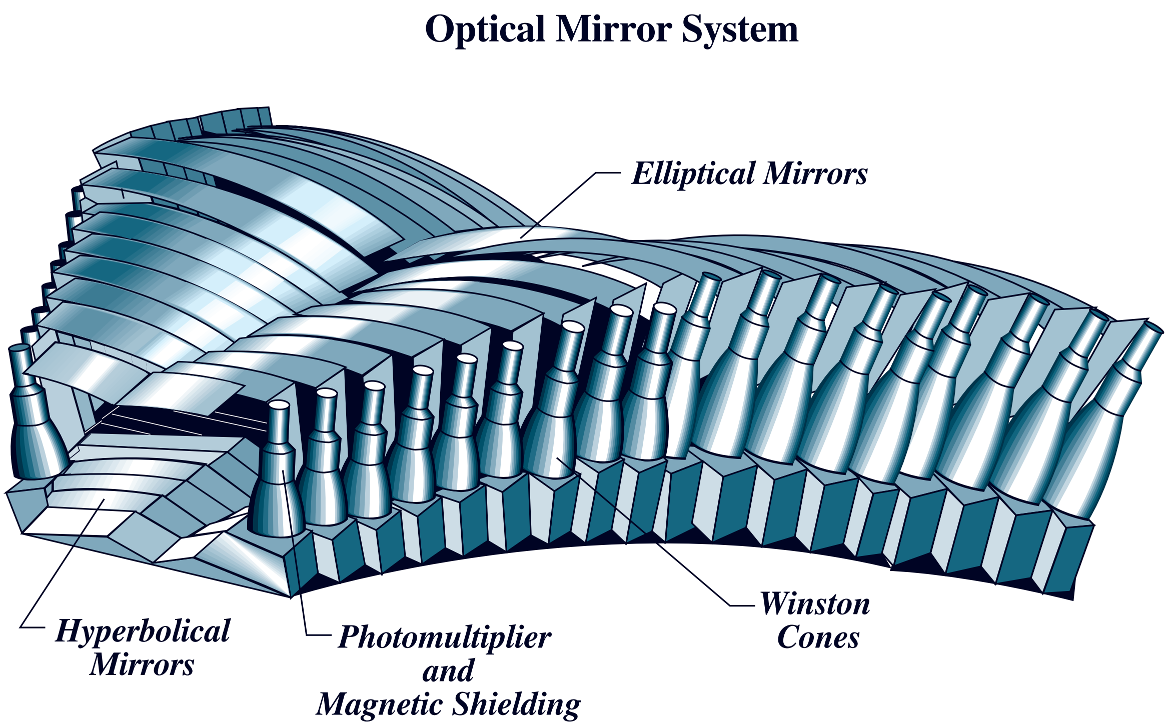

Fig. 3. A schematic drawing of the array of optical modules in one of six sectors.

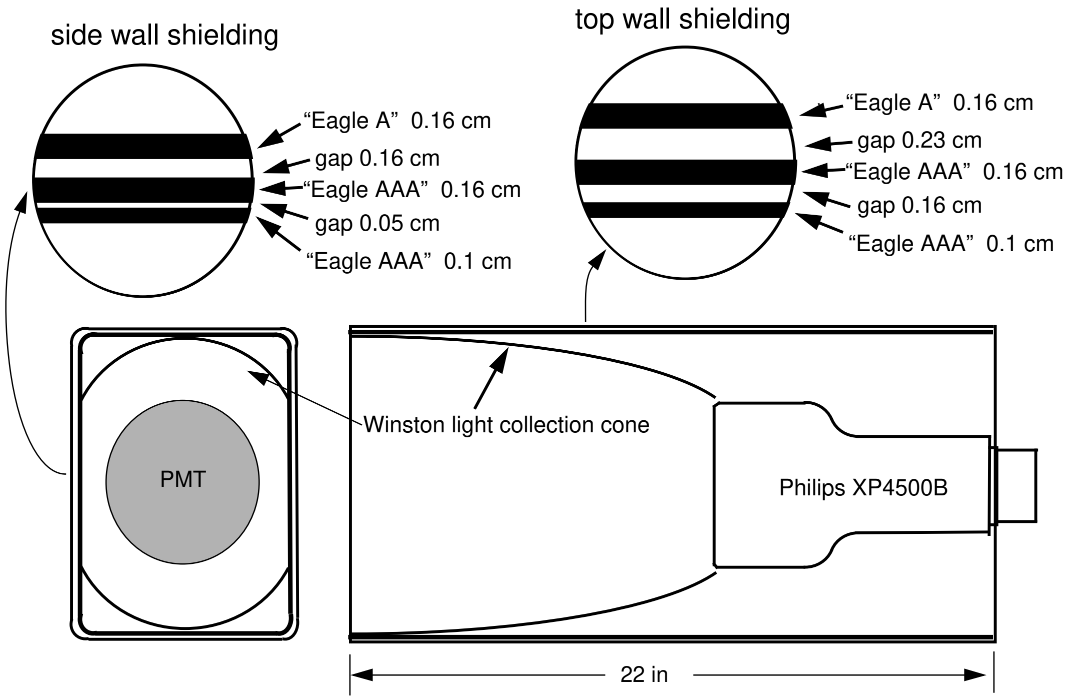

Fig. 4. PMT assembly with Winston light collection cone and magnetic shielding

on as few as one photolelectron, the single photoelectron peak has to be clearly resolvable, and as narrow as possible. Likewise, the photoelectron conversion efficiency should be as high as possible at as low wavelengths as possible, since much of the produced Čerenkov light is in the ultraviolet. Also, high photoelectron efficiency should extend over as large an area of the tube's face as possible, since the collected Čerenkov radiation is distributed smoothly over the face of the tube. Given the reflectivity characteristics of the mirrors, and the absorption with wavelength of the radiator gas, as well as budgetary constraints, the Philips XP4500B, with UV glass, proved to be the best match.

2.2 Magnetic Shielding

The photomultipliers are located in the fringe field region of the spectrometer coils. It was therefore necessary to surround each PMT with high permeability magnetic shields. The magnitude and angle of the applied magnetic field varies widely as a function of PMT position, with the highest fields located at large scattering angles. Computer simulations were used to design a shield that would accomodate components of the applied field up to 11 Gauss parallel to the PMT axis, and 70 Gauss transverse. A drawing of the magnetic shielding is shown in Figure 4.

The shields and Winston cones were produced in three standard sizes, with the smallest placed at the smallest θ-angle mirror assemblies and the largest at back angles. The PMT photocathode and first dynode are located near the center of each shield. The shields are formed in three layers of magnetic material, each having a rectangular cross section. The inner and middle layers are composed of high permeability alloy having a saturation induction of 8,500 Gauss (Eagle AAA). The outer layer material, of moderate permeability had a saturation induction of 21,500 Gauss (Eagle A). The thickness of the shielding materials and the separation gaps between the layers for the side and top walls of the shielding are indicated in the insets in Figure 4.

Bench tests of a prototype large-angle shield at maximum field showed an attenuation factor of 85 for the axial field and 390 for the transverse field at the photocathode position. Thus, an overall field strength less than 0.2 gauss is expected *in-situ*. Further tests with a pulsed photodiode were made to determine the detection effeciency of single photons when a shielded PMT is placed inside the spectrometer. The measured relative efficiency was about 95 percent at maximum field, but fell rapidly at higher applied fields due to saturation of the inner layers of the shield.

In order to understand the response of the complicated optical arrangement of the entire detector great effort was expended in developing an elaborate GEANT based design package [11] which simulated the details of the detector response for charged particles of various momenta and directions. The use of this package was essential in obtaining the optimum shapes and orientations of the various mirror componants.

2.3 Readout Electronics

The anode signals from the 216 photomultipliers are split in specially developed passive splitter modules. One of the split signals from each photomultiplier is fed into a leading edge discriminator, whose threshold is individually set using a programmable digital-to-analog converter unit to provide a timing signal. The discriminated signal is brought to a 64 channel FASTBUS time-to-digital converter module with 25psec least significant bit resolution. The other signal is brought to a FASTBUS 12 bit analog-to-digital converter. This information is used to determine the number of photoelectrons coming from the photomultiplier. The signal from the photomultiplier dynode provides a fast signal for the CLAS Level 1 trigger system. The Čerenkov ADC and TDC information is readout together with data from the other detector components using the the CEBAF Online Data Acquisition system (CODA).

2.4 Trigger Logic

The CLAS trigger system is designed as a two level system. The first level provides fast information from the electromagnetic calorimeter, the Čerenkov counter, and the time-of-flight scintillator system. This information must be available within 200 nsec. If the event is retained, a second level that uses information from the tracking chambers makes the decision whether the event should be recorded. During electron beam operation, the Čerenkov counter in coincidence with the calorimeter must provide the information whether the candidate event contains a scattered electron, and should be recorded.

The schematics of the trigger logic is shown in Figure 5.In the first step the signals from the left and right elements of each Čerenkov counter segment are linearly added in a specially-designed NIM module. This module also amplifies the signal by a factor of 10, minimizing detector inefficiencies for electrons entering the active volume near the detector midplane. Summing up the signals from the entire Čerenkov detector would increase the noise of the summed signal, and leave no flexibility for adjusting the Čerenkov trigger input into the CLAS Level 1 trigger system to accomodate specific physics requirements. Therefore it was decided to sum up the Čerenkov signal corresponding to portions of the detectors' active areas. This is accomplished by first summing up signals from four neighboring segments. The next sum of four segments overlaps two segments of the previous sum, *and so forth*. This prevents a loss of pulse height and avoids reduced efficiency for electrons that distribute their Čerenkov light to more than one detector segment. It also allows setting the trigger threshold to a higher level than would otherwise be possible if pulse height signals from individual segments were used. The number of segments included in the sums was determined by a Monte-Carlo simulation that included the full geometry of the detector. Only one event in 2000 had more than 4 segments collecting light from the simulated incident electron. The 18 detector segments in each sector are fully covered by 8 sums of 4 overlapping segments. In the next stage, the signals from each sum of four segments are split equally and fed into two leading edge CAMAC discriminator modules, whose thresholds are individually set using programmable digital-to-analog converter units. This allows a "low" and a "high" threshold to be applied. Events may then be selected according to a required minimum number of photoelectrons generated in the photomultipliers. The "high" threshold may be used to reduce the amount of "noise" triggers, while the "low" threshold may be used in a prescaled mode to provide unbiased information.

3 Construction

3.1 Mirror construction

Due to the detector's position upstream of the TOF scintillator array and electromagnetic calorimeters, the mirrors and their supporting framework are required to be as light as possible. In order to minimize the the nonuniform material distribution inherent in any supporting frame, the mirrors are constructed to be intrinsically rigid, as well as lightweight. This was

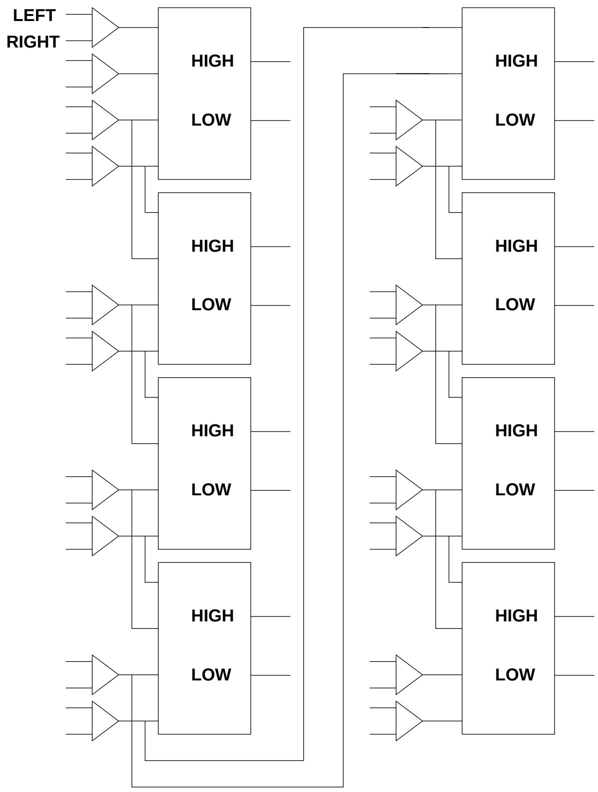

Fig. 5. Schematics of the trigger logic for use of the Čerenkov detector in the fast level 1 trigger.

accomplished by means of a multi-layered composite construction illustrated schematically in Figure 6. The mirror surface is aluminum, vacuum deposited [5], on a Lexan sheet [6] of thickness 0.76 mm, with a vacuum deposited surface layer of MgF_2 to prevent oxidation. This is laminated to a supporting structure consisting of three inner and three outer layers of Kevlar [9], with structural vinyl foam [10] sandwiched between to provide structural rigidity. The Kevlar fabric layers are of density 0.056 g/cm^2, with fibers of successive layers oriented in crossed directions to maximize tensile strength in all directions. Each mirror is supported at one end by an adjustable support frame, illustrated in Figure 3.1, which allows complete and independent spatial alignment.

A total of 432 elliptical and hyperbolic mirrors, having 36 different shapes, were fabricated as follows. An aluminum mounting surface having the preset shape of each elliptical or hyperbolic mirror is prepared with a PVC anti-bonding coating, followed by a sheet of nylon *peel-ply* [8] to facilitate release of the mirror after fabrication. The aluminized Lexan mirror substrate is placed on the mold, followed by the three inner layers of Kevlar impregnated with Epon epoxy [7]. A pre-formed sheet of structural foam was then placed upon the Kevlar. The foam's thickness is tapered down from the supporting end, shown schematically

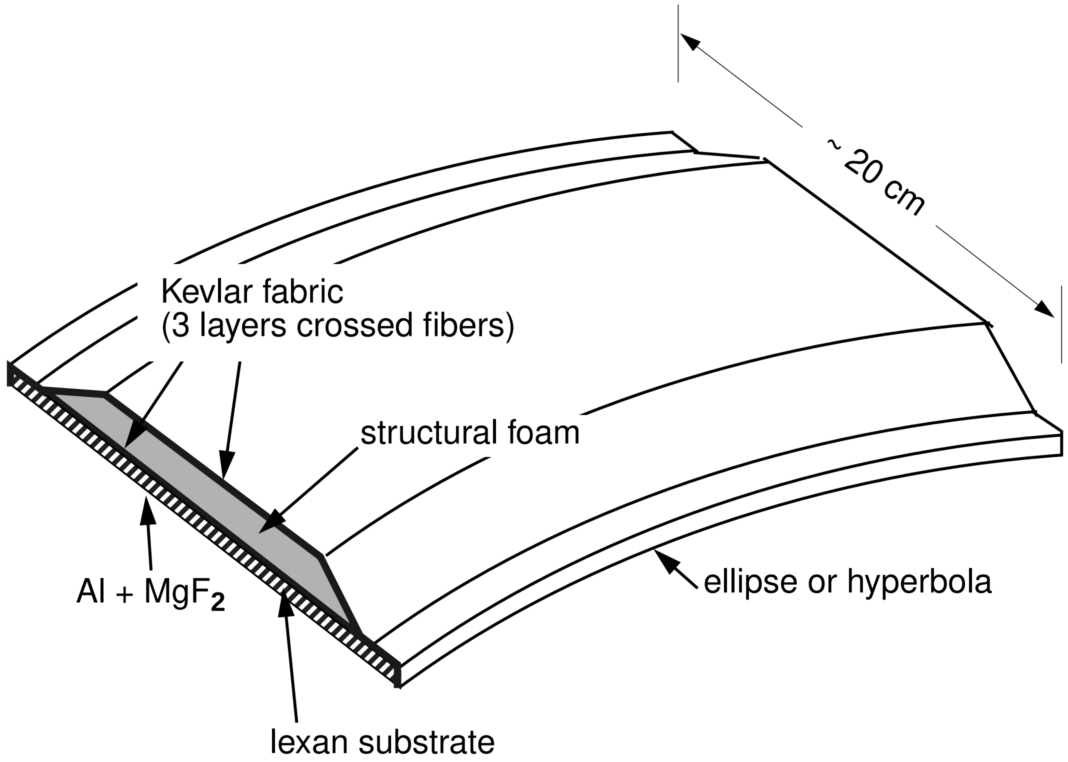

Fig. 6. The cross-section of a mirror used in the CLAS detector.

in Figure 3.1. The section at the supporting end has a wood inner layer rather than foam to facilitate the attachment of the mounting bracket, as shown in Figure 3.1. The foam is of a rigid consistency, which allowed us to pre-form its shape to the mirror curvature by heat treatment, before applying, thus reducing stress after cure. At this stage the structure was covered by plastic vacuum bagging, which was held to the mold and made vacuum-tight by applying a malleable adhesive, and evacuated so that the shape is maintained to that of the mold by air pressure. Cotton bleeder cloth is inserted prior to vacuum bagging to uniformly distribute the evacuation. After a 12 hour curing period the three outer Kevlar layers are mounted and again impregnated with epoxy. The entire structure is again evacuated and allowed to once more cure under vacuum for a period of 12 hours, after which the entire mirror assembly is removed and fitted with the supporting frame.

The mirror shapes were optically checked with a specially designed laser system. The reflectivity of the mirrors could not be measured directly due to the large size of a typical mirror assembly. However, small samples were cut from the mirror substrate material corresponding to that used for each individual mirror, and the reflectivity measured for these from the UV through the visible wavelengths. The measured mirror reflectivity are somewhat less than expected for an ideal aluminum surface though typically around 90% in the visible region, and smaller in the near UV (where much of the Čerenkov light is concentrated). The results of a typical measurement are shown in Figure 8.

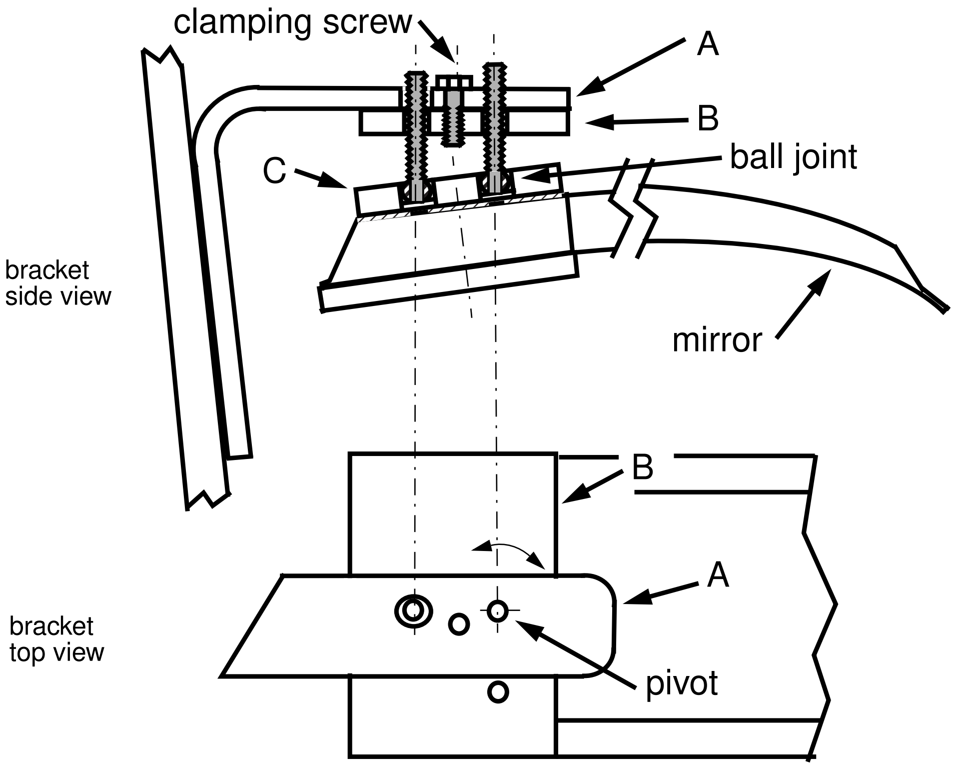

Fig. 7. Detail of the elliptical mirror used in the CLAS Čerenkov detector, showing the mounting/alignment bracket. The bracket used for the hyperbolic mirrors is similar.

The Winston cones used to collect the light onto the PMT surfaces are constructed with flat sides to accommodate close packing, as illustrated in Figure 4. For fabrication purposes the cones were standardized into three sizes, small, medium and large, of lengths 17, 21, and 29 cm, respectively. The small cones occupied modules 1 to 10 in each sector, the medium modules 11 and 12, and the large modules 13 to 18. The small and large cones were fabricated by an electro-forming process [12]. This was the most expensive of the various fabrication methods considered, but offered the best quality surface for mirror deposition, and had the least chance for deterioration over time. It also could be made thinner than with other techniques thereby minimizing the dead wall thickness presented to the reflected light. The copper cones were electro-formed, on pre-shaped steel mandrills, to a nominal thickness of 0.1 cm. The inner surfaces were vacuum coated with aluminum to a thickness of about 40 nm, followed by MgF_2. The small number (24) of medium cones were fabricated from plastic since the high overhead cost for manufacture of the steel mandrill made the cost per cone excessive. The 0.2 in thick plastic cones were formed by vacuum pressing onto hardwood mandrills, and then were vacuum coated with aluminum and MgF_2 similarly to the copper cones. The reflectivity of the cones was checked over the relevant wavelengths and only those passing acceptance criteria were retained. The most important factor leading to lower reflectivity was the nonuniform deposition of MgF_2 onto the inner surfaces.

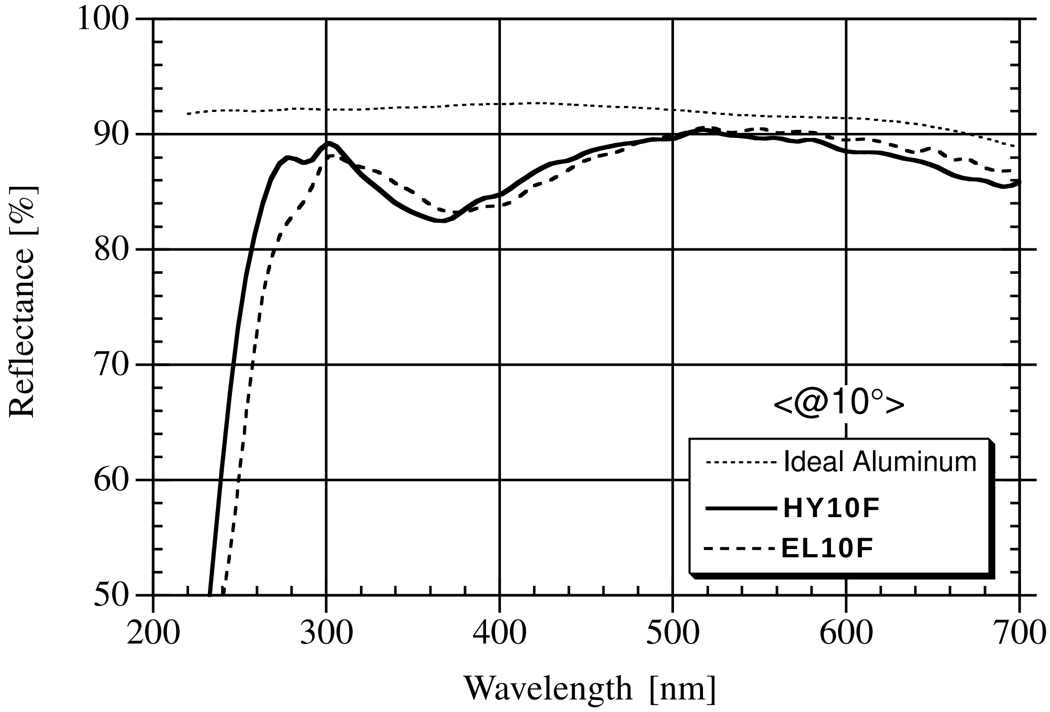

Fig. 8. Measured reflectivity as a function of wavelength for a typical sample of the mirror surface, which consists of Al and MgF_2 successively evaporated onto a substrate of 0.1 inch thickness Lexan sheet. The dotted curve is what would be expected of ideal aluminum. The solid and dashed curves are for the hyperbolic and elliptical mirrors respectively. The light was incident at an angle of 10° with the normal. Note the suppressed zero

3.2 Mechanical construction

Due to the six-fold symmetry of the CLAS spectrometer, the Čerenkov detectors were fabricated as six independent identical detector sectors. Each sector subtends an azimuthal angle (ϕ) of 60° and a zenith (scattering) angle $8 < \theta < 45°$. Each sector was individually assembled.

The superstructure on which all of the detector components, including mirrors, cones, shielding, phototubes and associated cables, were mounted consists of a three walled triangular shaped aluminum frame which forms the outer boundary of each sector.

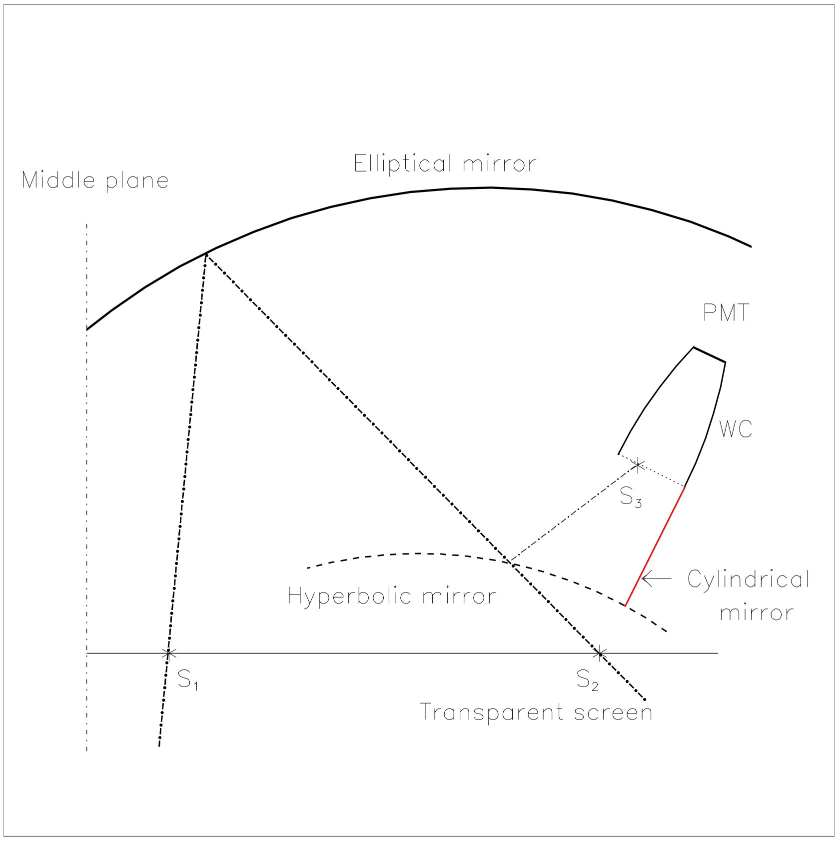

Fig. 9. Illustration of the alignment procedure. First the elliptical mirror is aligned so that the laser light from the target position reflects onto a pre-calculated spot on the mylar screen. Alignment of the hyperbolic mirror requires a secondary reflection onto the a predetermined point on a screen located at the face of the Winston light collection cone.

3.3 Mirror Optical Alignment

Due to the large size and weight of each module a special mounting fixture was constructed such that assembly and optical alignments were done with the framework positioned in the final orientation of the specific sector. This was done to minimize changes in optics due to changes in gravitational stresses for each orientation of the frame and optical elements during mounting. The assembly and alignment procedure follows.

- The Winston cones and cylindrical mirrors were attached to the magnetic shields, which were then mounted in their preassigned position on the frame walls. The three frame walls were then assembled, after which the 36 PMT's were inserted into the magnetic shielding units. This assembly was hoisted into the proper position and angle on the mounting fixture.

-The elliptical mirrors were inserted into the detector and aligned using a laser mounted at the putative target position. Figure 3.3 illustrates the alignment procedure. The three degrees of freedom were sequentially aligned by means of the specially designed screw-and-ball adjustments built into the mirror mounting brackets. The mirror alignment was performed by using the results of the ray-tracing simulation assuming that the Čerenkov light was emitted in exactly the same direction from the target as the electron, with magnetic field turned off so that the electrons would point back to the target. The light reflected from an elliptical mirrors intersects a predetermined coordinate on a transparent mylar screen as shown in Figure 3.3. The hyperbolic mirrors were then mounted, and aligned such that a subsequent reflection of the light from the aligned elliptical mirror was required to intersect a predetermined coordinate on a screen at the entrance to the light collection cone. After alignment, the standard deviation of the distribution of the light on the face of the Winston cone after being reflected from various points on the mirrors, was typically about 1 cm, corresponding to an angle of about 1.5 mr. Finally, the elliptical mirror alignment was fixed by permanent attachment with epoxy to a lightweight spine at the midplane of the sector.

3.4 Gas Containment Windows.

After the mirrors were aligned the detector was removed from the alignment fixture and the gas containment windows were attached. The windows consist of two laminated sheets of .08 mm Tedlar [13] PVF film sandwiched around a sheet of mylar. Tedlar was chosen because of its high strength, durability, and opaqueness to light. The window was glued onto the detector walls in a manner which minimizes gas leaks. This was a rather complicated procedure since the windows are not rigid, and the joints with the detector walls must withstand significant forces due to the weight of the C_4F_{10} gas. The gas density of C_4F_{10} is about 9.94 kg m^{-3}. Since each sector has a volume of about 6 m^3, the total mass of gas in a sector is about 60 kg, so that the pressure at the joints can be as high as 500 Pa, with transient variations as high as $\pm$ 200 Pa due to variations in external air pressure and ambient temperature. Finally, thin Kevlar sheets, which were securely fastened to the detector frame, covered the entire window area. This was vital to help relieve pressure stresses on the leak-tight window-frame joints. Leak rate, variations in atmospheric temperature pressure and ambient temperature are monitored continuously.

3.5 Gas System

C_4F_{10} (perfluorobutane) was chosen as the radiator gas for its high index of refraction ($n = 1.00153$), which results in a high photon yield, and an acceptably high pion momentum threshold of $p_\pi \sim 2.5\,\mathrm{GeV}/c$. In addition,$C_4F_{10}$ has excellent light transmission properties. The minimum cutoff wavelength for C_4F_{10} is about 190 nm compared to Freon-12 which is about 230 nm. The measured mirror reflectivity, though typically around 90 % in the visible region, drops to about 85% in the near UV, and then typically near 20% at 200 nm, so that

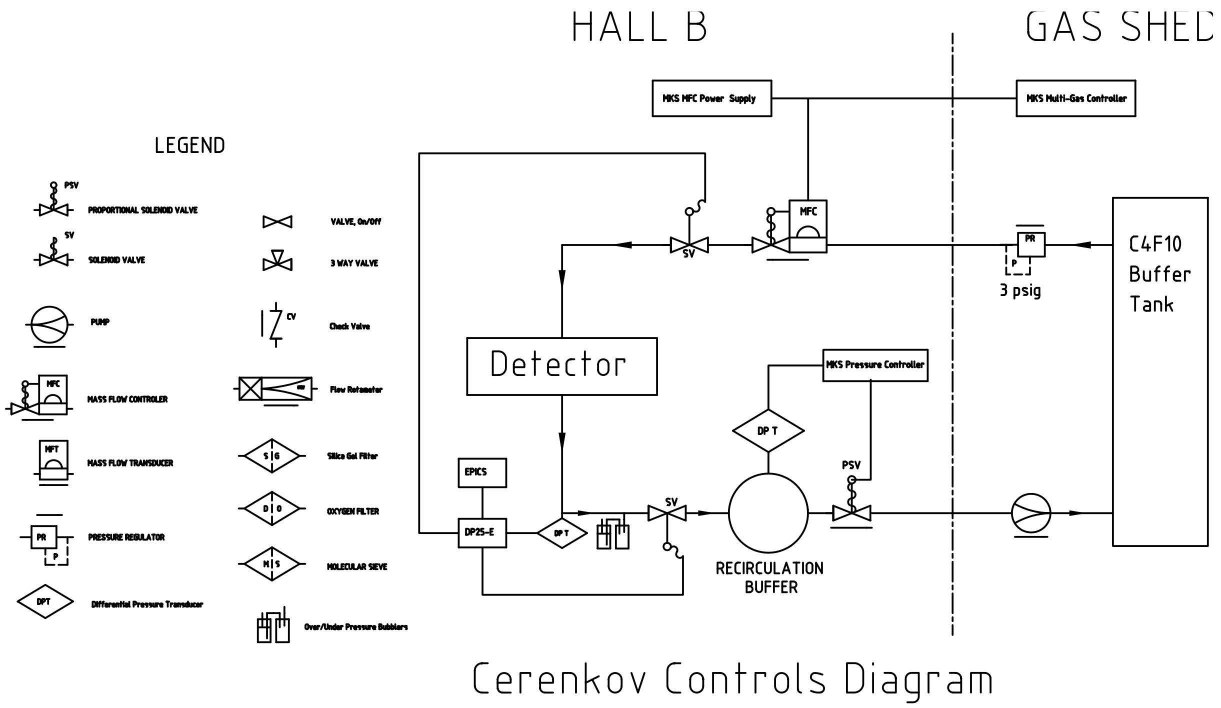

Fig. 10. Schematic of the Čerenkov gas system.

light absorption in gas does not play a significant role in degradation of signal.

Each sector of the detector holds about six cubic meters of gas. The cost of gas for one volume of detector is about \$30K. With very large large joints where the flexible window attaches to the detector frame, great efforts were employed to minimize gas leaks (see previous section). The physical density of the gas is about 9.94 kg/m^3, which corresponds to a maximum net pressure of about 340 Pa. Thus, even small leaks result in significant leakage. Finally a leak rate of about one volume per two years was found to be acceptable.

This gas is supplied to the detector with a gas system built specifically for this purpose. The requirements for such a gas system are that it must be able to recirculate the gas through the detector, maintain an approximately constant pressure within the detector, and remove impurities from the gas. Figure 10 shows a schematic of the gas system.

Oil bubblers are installed on each sector individually to protect the sector from either an over-pressure or an under-pressure situation. In the event of an overpressure state, C_4F_{10} is vented to the atmosphere. In an under-pressure condition, air is sucked into the detector. The gas system is designed to run automatically, altering the flow into and out of the sectors to accommodate changes in external air pressure, with minimal human intervention. Periodic monitoring of the pressure differentials within each sector are sufficient to ensure proper functioning of the system.

4 Photomultipler Studies

Measurements of photomultiplier quantum efficiency and photocathode uniformity was accomplished on a custom optical bench designed for the express purpose of performing optical measurements of interest for detector design and testing within the JLAB nuclear physics community. It is built upon a standard 4×6 feet industrial lab bench with a sturdy wooden top. A wooden enclosure (open at the bottom) was built to sit upon the benchtop thereby creating a dark interior (with all relevant interior surfaces painted flat black). The enclosure was mounted on four pneumatic cylinders so that it could be raised up almost 1 m above the benchtop and allow access to the test apparatus. The dark box was a requirement as most of the relevant measurements involved the use of highly sensitive photodetectors designed for very low ambient light levels. The main mode of testing involved DC measurements of optical response as a function of wavelength. In accordance with this, a standard set of equipment included a UV/VIS broad-band light source (75W xenon lamp), a UV/VIS monochromator, an integrating sphere and a UV/VIS photomultiplier. The monochromator manufacturer [24] provided a data acquistion module for computer control of the monochromator wavelength setting and for measurement of the photomultiplier current (with a range of 0.01 nA to 0.1 mA). The data acquisition module was connected via RS-232 to a DOS PC. A user-written MS QuickBasic program was used to control the data acquisition. Associated equipment included lenses, collimators, a silica fiber bundle, filter wheel (with narrow-band and neutral density filters), and a XY scanner to allow for precision positioning of test components. Quantum efficiency (QE) was measured by comparing the response of a sample XP4512B phototube to the measured responses of three different calibrated phototubes. Care was taken to illuminate the entire photocathode with the source light. The manufacturer of the test PMT provided a measure of the QE at 400 nm. Combining this with the measured wavelength responses of the test vs the calibrated PMTs allowed one to calculate the QE for the test PMT. The use of 3 calibrated phototubes allowed one to estimate the errors. Figure 11 displays a typical example of this data.

These tests also verified that some of the early samples of the phototube used a poorer grade of faceplate leading to insufficient QE at the important UV wavelengths where the Cerenkov spectrum is maximized. Uniformity of response across the photocathode was measured by focussing light (via a silica optical fiber bundle attached to a focussing lens couplet) into a 5 mm spot on the phototube faceplate. The PMT was mounted on a XY scanner which allowed for a raster scan of the PMT photocathode. An example of the DC response (at a typical gain of 2×10^7) for a wavelength of 400 nm is shown in fig. 12. The central bump is directly above (and due to) the dynode chain. The substantial dip in response across the left half corresponds to a previous observation [25] for this same model of phototube. Analysis by the manufacturer indicated that it is due to a gain drop across the second dynode [25]. Large variations in PMT uniformity (other than this previous dip) were only observed for wavelengths above 600 nm and so were not a problem for this UV-VIS Cerenkov detection

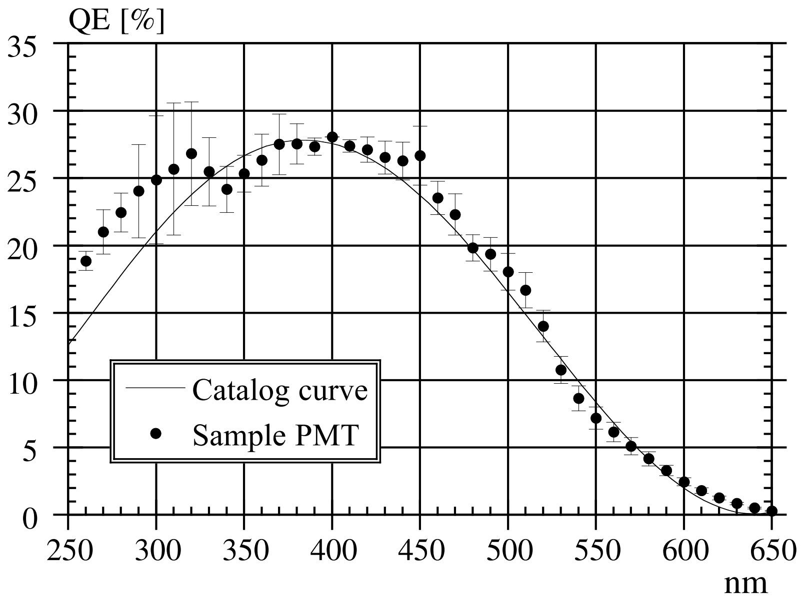

Fig. 11. Typical quantum efficiency data from a selected sample of XP4512B phototubes.

application.

5 Photomultiplier Calibration

The calibration of the CLAS Čerenkov detector consisted of matching the gains of the 216 PMTs. The main reason for this is so that the discriminator threshold has the same cutoff for each PMT. This was accomplished by taking a set of special runs in which the data acquisition system was triggered on the PMT noise within the Čerenkov detector, and only the Čerenkov data was written to file. Because the PMTs have different noise rates, from a few hundred Hz to several kHz, several runs were necessary, in between which the noisier PMTs were turned off.

After all the data was collected, the ADC spectrum for each PMT was fit to a function of the form

$$A(x) = T\left(A_{noise}(x) + A_{SPE}(x)\right) \tag{1}$$

$$A_{noise}(x) = C_1 e^{-C_2 x} \tag{2}$$

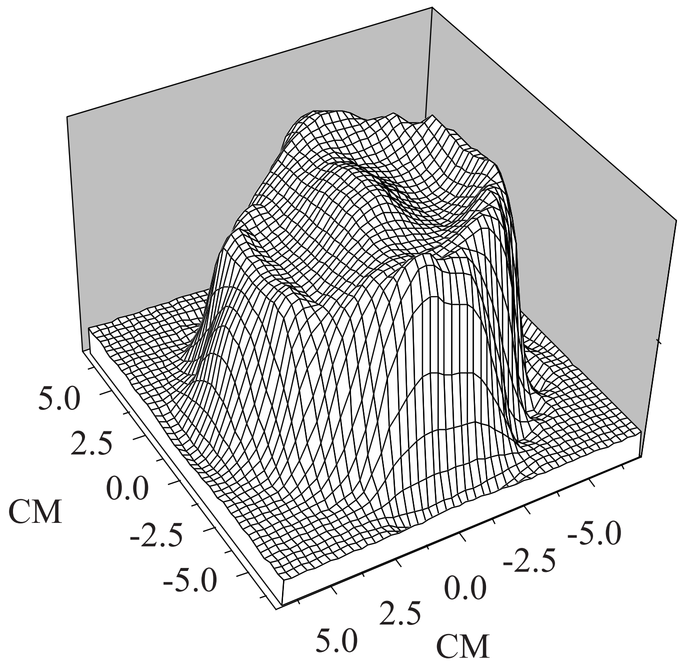

Fig. 12. Typical response of XP4512B across the photocathode. As noted in the text, a major factor in this response curve is the gain behavior of the dynode chain, in particular the second dynode [25].

$$A_{SPE}(x) = C_3 e^{-(x-C_4)^2/C_5^2} \tag{3}$$

where $C_1 - C_5$ are fit constants, and T is a modified step function, smeared to account for the effect of the discriminator threshold. This function presumes that the two main components of the lineshape correspond to electronic noise (A_{noise}) and the single photoelectron peak (A_{SPE}). A typical ADC spectrum is shown along with the fit function in Fig. 13. Using the fit parameters, specifically C_4, which corresponds to the position of the SPE peak, we can adjust the high voltage on the PMT to move the SPE peak into a particular channel.

During the course of the first data run, it was determined that the gains of several of the phototubes drifted with time. To alleviate the trouble that could potentially cause for the data analysis, several calibration runs were taken during the course of the first production experiment. By monitoring the gain drift over time, we can get a good idea of its effect on our data.

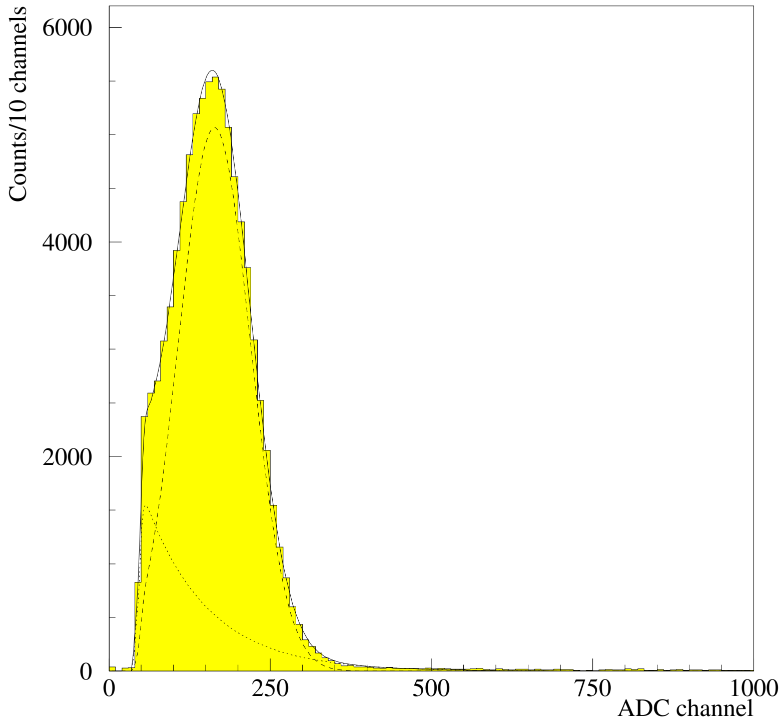

Fig. 13. A typical ADC spectrum showing the single photoelectron peak (dashed line) and the electronic noise (dotted line). The solid curve shows the sum of the two separate components.

6 Performance

6.1 Fiducial Volume and Efficiency

In order to calculate absolute cross sections, both the fiducial volume of the CLAS and the detector efficiency within that volume must be established. Because of the open geometry of the CLAS, particles can trigger the detector at the extreme edges of the acceptance, where the detector efficiency may not be well understood. Therefore, the fiducial boundary which defines 'good' acceptance must be carefully determined for each detector component, in order to produce a well-defined solid angle and minimize large efficiency corrections.

For the Čerenkov detector, this boundary is defined by the edges of the mirrors, beyond which the optical collection efficiency for Čerenkov light rapidly drops. This efficiency was studied *in situ* using elastic scattering of electrons from a hydrogen target. The strong kinematic correlation between scattering angle and momentum for elastic events creates a one-to-one correspondence between the electron's azimuthal and polar angles at the target, (θ, ϕ), and the entry point of the electron on the surface of the Čerenkov detector.

Elastically scattered electrons are selected by kinematical cuts, and a match between a reconstructed track and a reconstructed shower in the electron calorimeter. A cut on the invariant mass of the hadronic final state, $W^2 = (E - E')^2 - (\vec{P} - \vec{P}')^2$, is used to select elastic events.

The Čerenkov inefficiency as determined from the measured photoelectron yield is plotted in Fig. 14. Here variations in the optical collection efficiency associated with the individual mirror segments are apparent. However except for isolated spots at the midplane, where the gaps between mirrors are largest the electron efficiency within the fiducial acceptance should exceed 99%.

Outside of the region of high optical collection efficiency, the photoelectron inefficiency increases rapidly, and this region must be excluded using fiducial cuts. Using only the events within this fiducial boundary, we have calculated raw elastic cross sections, shown in Fig. 15. These show deviations from the expected dependence that are no greater than $\pm 5\%$, except at the smallest angles ($\leq\ 22^o$), where the fiducial cut extends beyond the edge of the forward-most mirror.

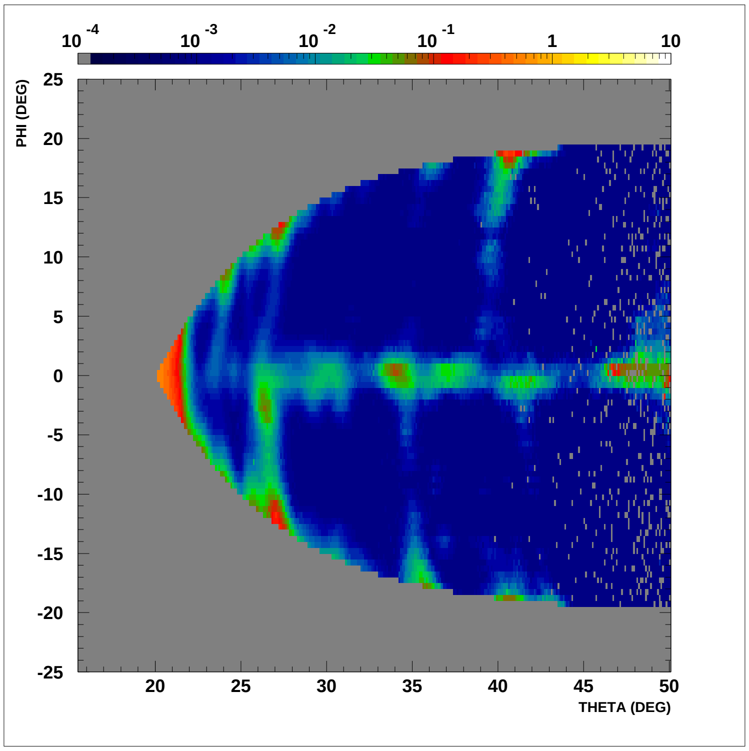

Fig. 14. Acceptance of the CLAS Čerenkov detector measured using 1.6 GeV electrons elastically scattered from protons. Plotted are scattering angles θ and ϕ defined with respect to the beam-line. The inefficiency (1-efficiency) is plotted according to the color scale at the top of the figure. The number of events/bin is logarithmically weighted according to the color scale at top. The dark blue regions which dominate the plot correspond to between 0.001 and 0.02. The sharp edges correspond to the software fiducial cuts discussed in text. For this measurement the magnetic field was set to 60% of its maximum value. The scattering angles θ and ϕ are defined with respect to the beam-line.

References

[1] D.S. Carman et al, Nucl. Instr. and Meth. in Phys. Res. **A419**, 315 (1999); Nucl. Instr. and Meth. in Phys. Res. **A449**, 81 (2000). M. Mestayer.

[2] E.S. Smith et al., Nucl. Instr. and Meth. in Phys. Res. **A432**, 265 (1999).

[3] To be published.

[4] Eagle Magnetic Co., Indianapolis, IN 46224.

[5] Liberty Mirror Co., Breckenridge, PA 15014

[6] Cadillac Plastics and Chemical, Albany, NY. distributer:Curbell Industrial Plastics

[7] Epon type 828 epoxy.)

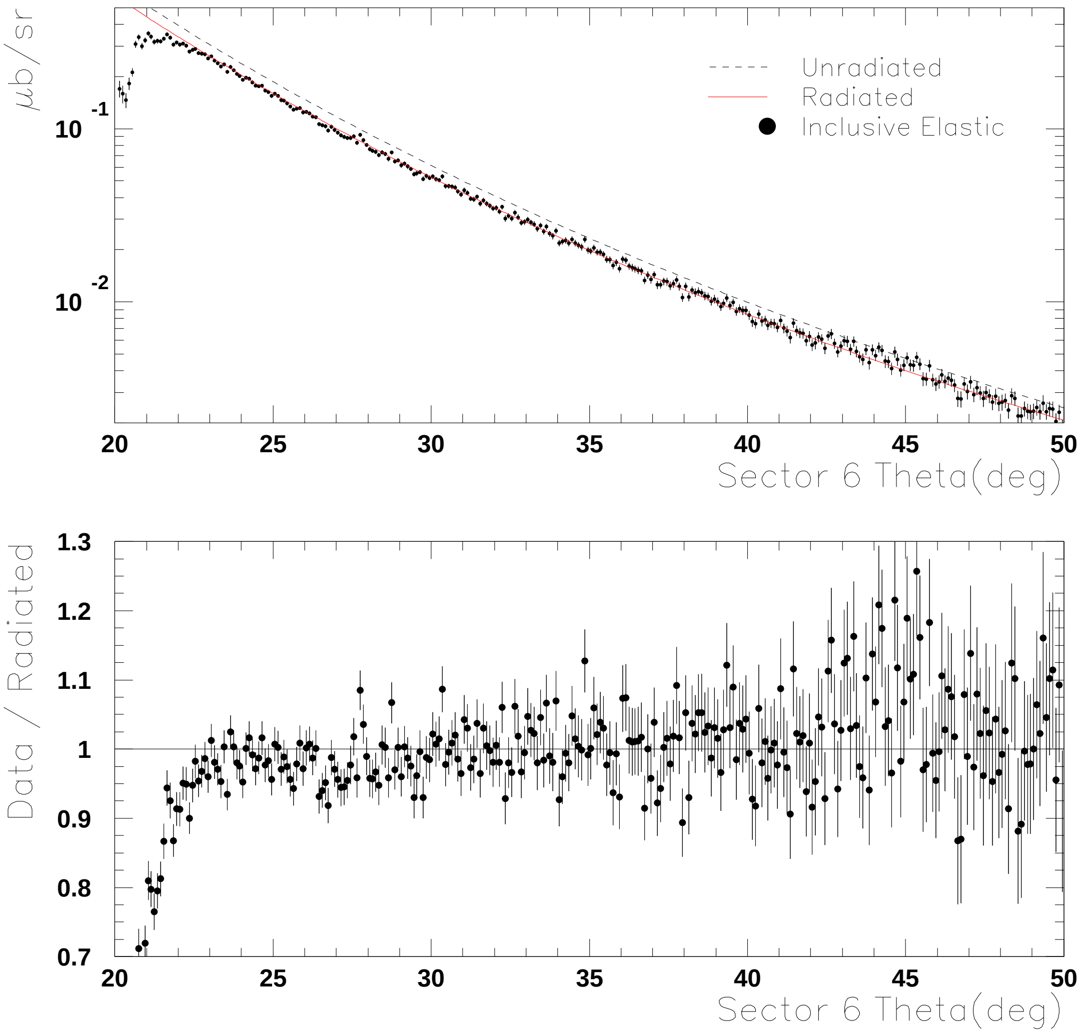

Fig. 15. Top. Measured cross section for $ep \to ep$ elastic scattering at beam energy of 1.645 GeV. Fiducial cuts for Čerenkov detector shown in Fig.14 are used to define the solid angle for each θ bin. No corrections for Čerenkov efficiency were made. The curve labeled 'Radiated' denotes the Rosenbluth formula, radiatively corrected according to Mo and Tsai [26], with the elastic form factor parameterization of Bosted [27].
Bottom: The ratio of the radiatively corrected measured cross section to that calculated with the Rosenbluth formula.

[8] Fiber Glast Developments Corp., Dayton OH 45414.

[9] Fiber Glast Developments Corp., Dayton OH 45414.

[10] Klegecell type 75 and 45 structural foam. Polinex, Grapevine TX 76051.

[11] CERN Program Library Q123, JLAB CLAS note.

[12] Optical Radiation Corporation, Azuza CA 91702.

[13] Tedlar PVF film: Dupont, Wilmington, DE 19898.

[14] To be published elsewhere.

[15] Particle data group

[16] Zrelov , Cherenkov radiation in high energy physics

[17] Jelley , Cerenkov radiation and it's application

[18] Nucl. Instr. and Meth. **138**, 641 (1976).

[19] Nucl. Instr. and Meth. in Phys. Res. **A248**, 118 (1986).

[20] Nucl. Instr. and Meth. in Phys. Res. **A343**,74 (1994).

[21] Nucl. Instr. and Meth. in Phys. Res. **A343**, 268 (1994).

[22] Nucl. Instr. and Meth. **93**, 593 (1971.)

[23] PCR Inc. P/O box 1466 Gainesville, Florida. 32602 - 1466 phone (904) - 376 - 8246 Fax: 371-6246 .

[24] manufacturer: Jobin Yvon / Horiba, Inc., Edison, NJ.

[25] M. Moszynski et al., Nucl. Instr. Meth. **A307**, 97 (1991).

[26] L.W. Mo and Y.S. Tsai, Rev. Mod. Phys., **41**, 205 (1969).

[27] P.E.Bosted, Phys. Rev. **C51**, 409 (1995).